Supplementary information

Electron tomography analysis of 3D interfacial nanostructures appearing in annealed Si rich SiC films

Ling Xie,[a] Karol Jarolimek,[b] Rene A. C. M. M. van Swaaij,[b] Vancho Kocevski,[c] Jan Rusz,[c] and Klaus Leifer*[a]

a. Applied Materials Science, Uppsala University, Ångströmlab, Lägerhyddsvägen 1, 752 37 Uppsala, Sweden; E-mail: klaus.leifer@angstrom.uu.se
b. Photovoltaic Materials and Devices, Delft University of Technology, Mekelweg 4, 2628 CD Delft, The Netherlands
c. Materials Theory Division, Uppsala University, Ångströmlab, Lägerhyddsvägen 1, 752 37 Uppsala, Sweden

1. The size of the c-Si and 3C-SiC NPs in 15 minutes annealed SRSC film

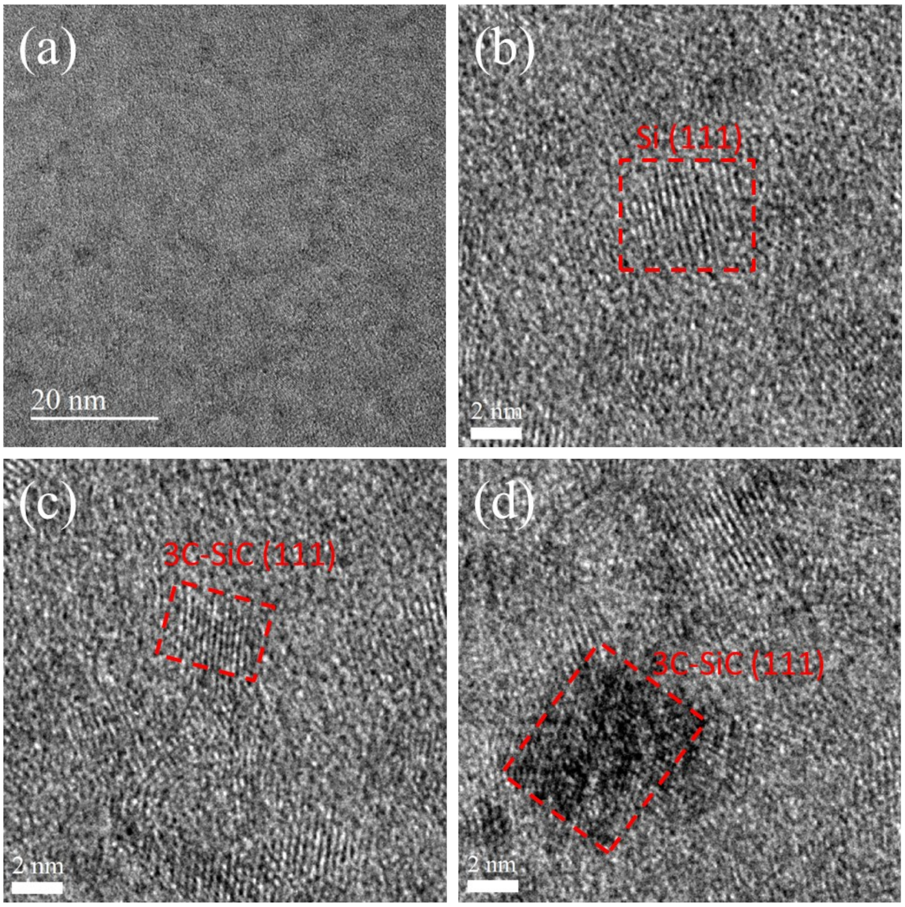

Fig. S1. HRTEM images of 15 minutes annealed SRSC film. In (a), the dark dots like contrasts were observed in an overview image indicating the presence of crystalline NPs after 15 minutes annealing. In (b), a 5 nm 3C-SiC NP was identified by showing the 3C-SiC (111) lattice fringes. In (c), a 4 nm Si NPs was identified by showing the Si (111) lattice fringes. In (d), a 10 nm 3C-SiC NP was identified by showing the 3C-SiC (111) lattice fringes.

The crystalline Si (c-Si) and 3C-SiC NPs were identified by measuring the spacing of lattice fringes. In Fig. S1a and d, the measured lattice fringe spacing is 2.53 ± 0.04Å, thus it is corresponding to 3C-SiC (111) lattice plane spacing. Similarly, the c-Si NPs were identified using the same method, in Fig. S1b, the measured Si lattice fringes spacing is 3.18 ± 0.03 Å which corresponds to Si (111) lattice plane spacing.

The size of c-Si NPs were measured from the HRTEM images by selecting 36 c-Si NPs. The average size of Si NPs is about 5 nm after 15 minutes annealing, one 5 nm Si NP was shown in (b). One 4 nm 3C-SiC NP was shown in (c) and one 10 nm 3C-SiC NP was shown in (d).

2. The determination of the Si plasmon peak position by considering the size effect of the c-Si NPs in 1 hour annealed SRSC film

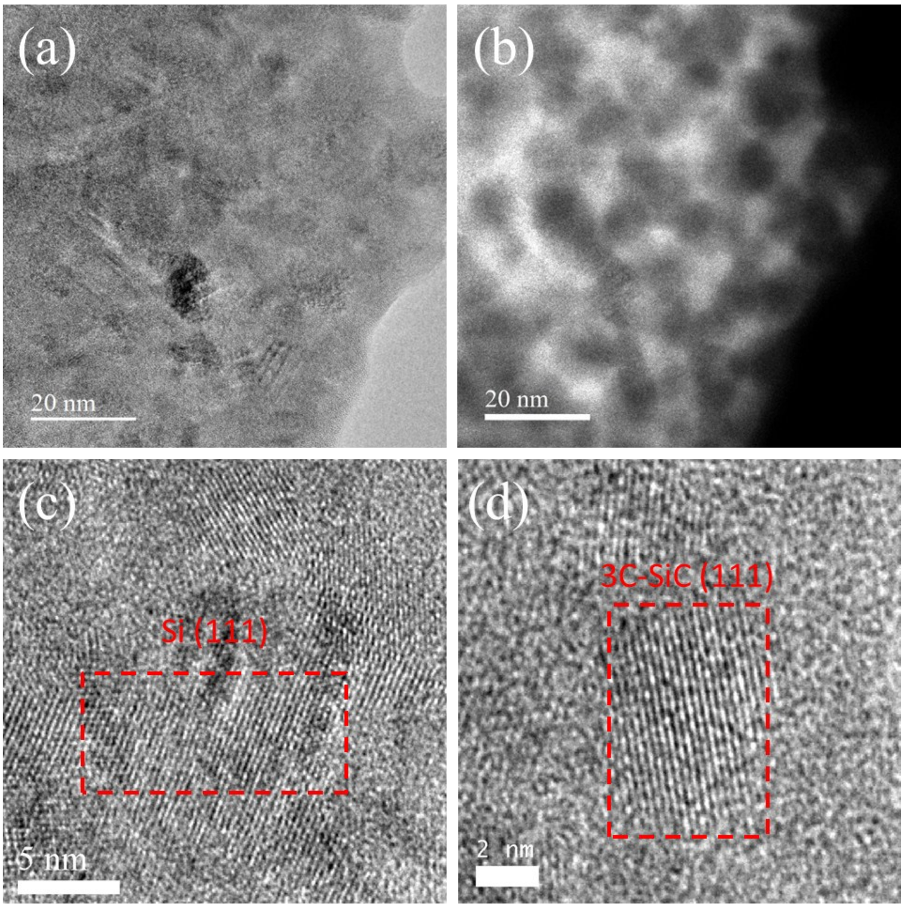

Fig. S2. TEM images of 1 hour annealed SRSC film. In (a), the dark dots like contrasts were observed in BFTEM image indicating the crystalline NPs after 1 hour annealing. In (b), it is the Si plasmon image. The typical size of the Si features ranges from 7 nm to 18 nm. In (c), a 5 nm X 12 nm Si NPs was identified by showing the Si (111) lattice fringes. In (d), a 7 nm X 10 nm 3C-SiC NP was identified by showing the 3C-SiC (111) lattice fringes.

The c-Si and 3C-SiC NPs were identified by measuring the spacing of lattice fringes. In Fig. S2d, the measured lattice fringe spacing is 2.54 ± 0.04 Å, thus it is corresponding to 3C-SiC (111) lattice plane spacing. Similarly, the c-Si NPs were identified using the same method, in Fig. S1c, the measured Si lattice fringes spacing is 3.18 ± 0.04 Å which corresponds to Si (111) lattice plane spacing.

The center of the Si plasmon peak can be affected by the size of c-Si NPs due to the quantum confinement effect [1]. The size of c-Si NPs can be assessed from the HRTEM images as shown in (a). In (a), both c-Si and 3C-SiC NPs can be identified by measuring the lattice fringes seen from the HRTEM image. (b) is the Si plasmon image showing the 2D projection of the network like structure. The triple junction areas show as the dominant contrast with a typical size ranging from 7 nm to 18 nm. In (c), from the HRTEM image, a c-Si NP was identified by showing Si (111) lattice fringes. It has a very irregular morphology with a size of 5 nm X 12 nm. After 1 hour annealing, the c-Si NPs measured from the HRTEM images have a size above 5 nm which indicates that the plasmon peak contributed from the c-Si NPs should not shift to the higher energies than 17.2 eV, because the c-Si NPs smaller than 5 nm have the higher plasmon energies than 17.2 eV [1]. Thus, the center of the Si plasmon peak should be located between 16.5 eV (16.4 eV is corresponding to a-Si) and 17.2 eV, since a significant amount of a-Si remains after 1 hour annealing (in Fig. S9, Raman analysis) and the Si plasmon peak is constituted by both a-Si and c-Si phases.

3. The determination of the fitting parameters for Si, a-SiC and 3C-SiC plasmon peaks

The centers of the plasmon peaks for a-SiC and 3C-SiC were adopted from the documented values, at 20 eV [2] and 22.5 eV[2] respectively. The Si surface plasmon energy was calculated under the free electron approximation using the formula [3]: $E_s = E_p/\sqrt{2}$. Thus, the center of the Si surface plasmon energy was fixed at 12 eV. From the previous studies, the volume plasmon energies chosen for imaging Si NPs embedded in SRSO or SRSC were at either at 17 eV or 17.5 eV. In our case, the measured size of c-Si NPs from HRTEM images (discussed in last section) is above 5 nm, and a significant amount of a-Si was observed from Raman analysis for 1 hour annealed SRSC film, thereby it is reasonable to assume that the Si plasmon peak is located between 16.5 eV and 17.5 eV. A series of tests were performed to find out the center of Si plasmon peak and the FWHM of each plasmon peak.

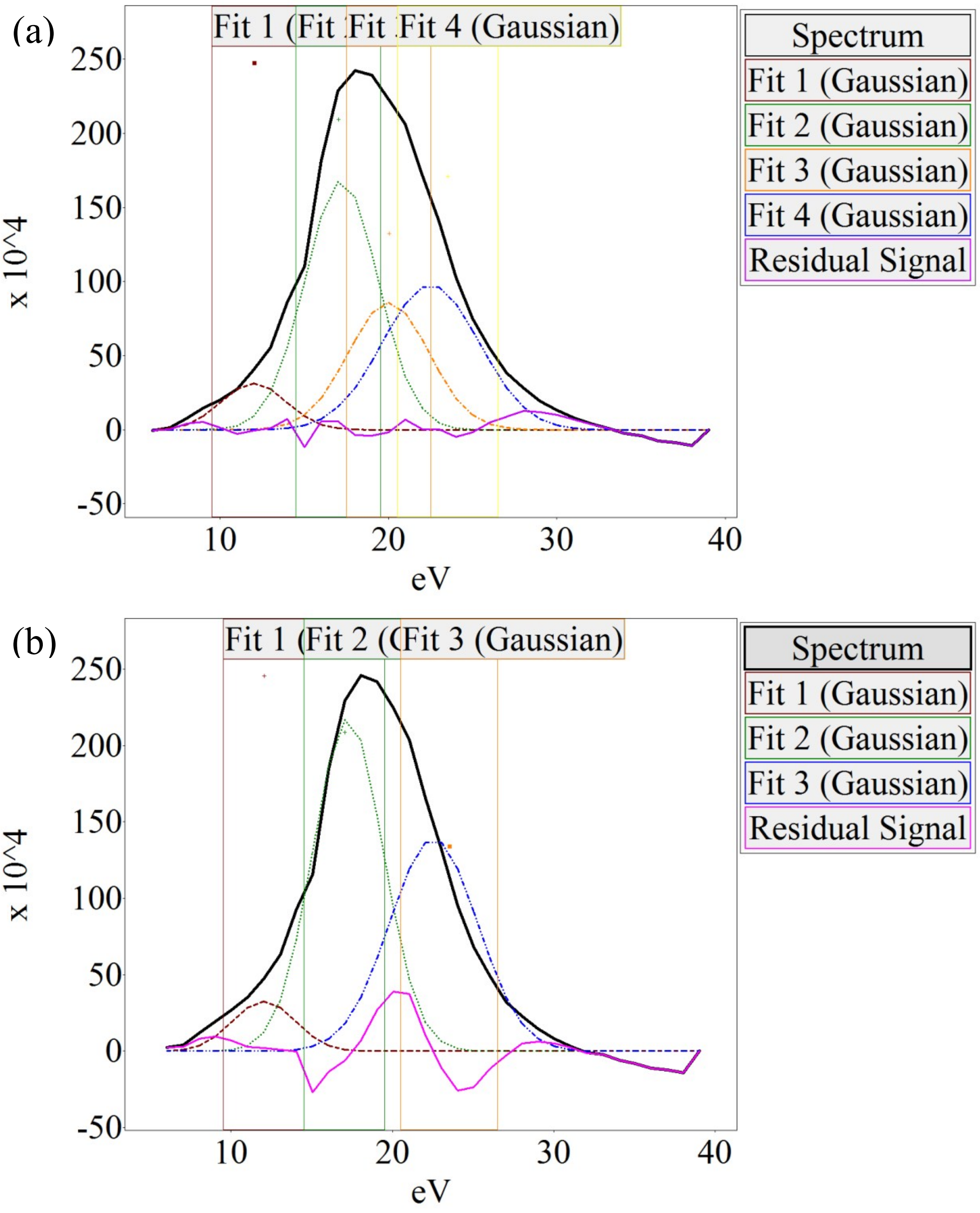

Fig. S3. The comparison between the fittings using 4 Gaussians and 3 Gaussians. In (a), the centers of the Si surface plasmon, Si plasmon, a-SiC plasmon and 3C-SiC plasmon peaks were fixed at 12 eV, 17.2 eV, 20 eV and 22.5 eV respectively. They were represented by the Gaussians 1, 2, 3 and 4 respectively in (a). In (b), the centers of the Si surface plasmon, Si plasmon and 3C-SiC plasmon peaks were fixed at 12 eV, 17.2 eV and 22.5 eV respectively. The Gaussians 1, 2 and 3 in (b) are corresponding to Si surface plasmon, Si plasmon and 3C-SiC plasmon peaks. In (a) and (b), the FWHM of 3C-SiC plasmon peak was constrained to be 6.5 eV [2]. All other plasmon peaks are not constrained by FWHM in (a) and (b).

In (a), the background extracted low-loss region can very well fitted with 4 Gaussians from 5 eV to 26 eV with a residual signal less than 4% of the total intensity. At about 28.5 eV, the residue plasmon signal was observed and considered as carbon. The FWHM for each plasmon peaks obtained from (a) are: Si surface plasmon: 4.5 eV; Si: 5.1 eV; a-SiC: 5.6 eV; 3C-SiC: 6.5 eV. If the centers of Si surface plasmon, Si plasmon, a-SiC plasmon and 3C-SiC plasmon peaks are fixed and all the FWHM of plasmon peaks are not constrained, then the fitting was shown in Fig. S4. The FWHM of 3C-SiC is 12 eV and the intensity of 3C-SiC plasmon peak is too low. It is not a good fitting shown in Fig. S4.

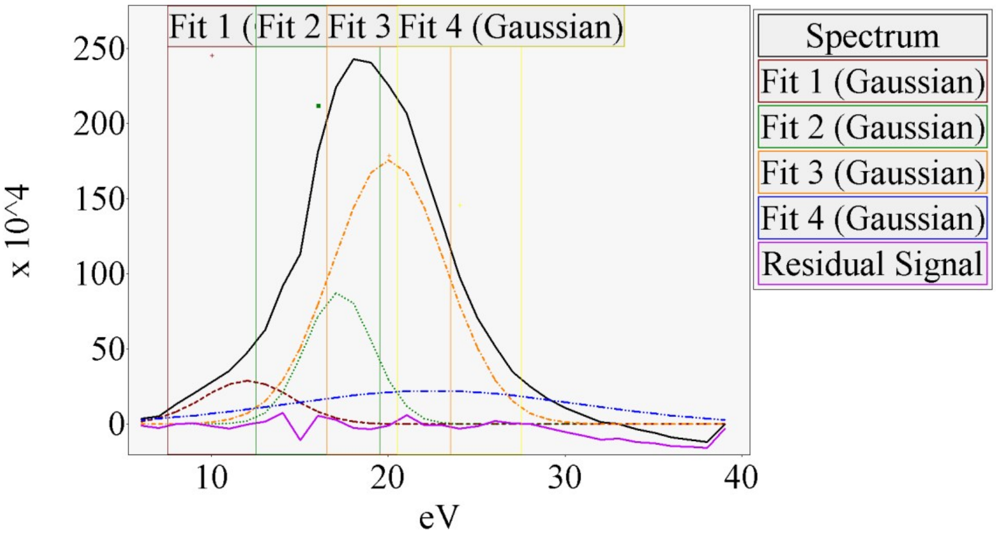

Fig. S4. The fittings using 4 Gaussians with only fixed centers of plasmon peaks. The centers of the Si surface plasmon, Si plasmon, a-SiC plasmon and 3C-SiC plasmon peaks were fixed at 12 eV, 17.2 eV, 20 eV and 22.5 eV respectively. The FWHM of all peaks are not constrained.

In Fig. S3 (b), it demonstrates that the a-SiC plasmon peak must be added in order to have a reasonable fitting. When the a-SiC plasmon peak was taken away, then a residual signal raised at 20 eV becomes pronounced.

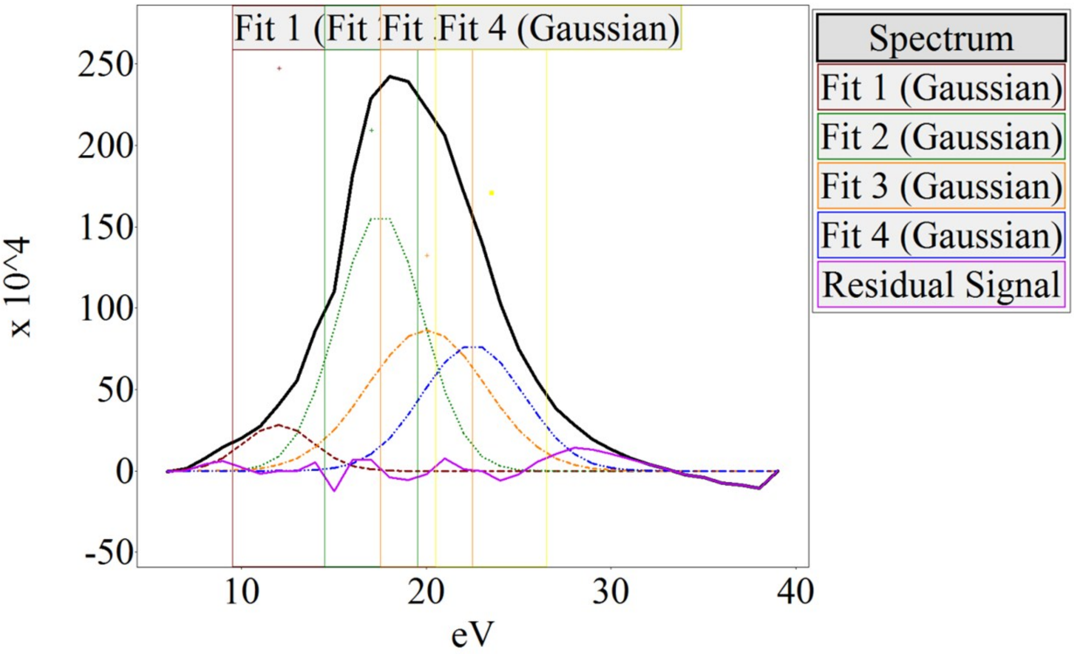

Fig. S5. The fitting results by shifting the center of Si plasmon peak to 17.5 eV. Si surface plasmon, Si plasmon, a-SiC plasmon and 3C-SiC plasmon peaks were represented by the Gaussians 1, 2, 3 and 4 respectively. The centers of Si surface plasmon, Si plasmon, a-SiC and 3C-SiC plasmon peaks were fixed at 12 eV, 17.5 eV, 20 eV and 22.5 eV respectively. The FWHM of 3C-SiC plasmon peak was constrained by 6.5 eV and the FWHM for all other plasmon peaks were not constrained in order to achieve minimum residual signal. The fitted FWHM of Si surface plasmon, Si plasmon and a-SiC plasmon peaks are 4.5 eV, 5.4 eV and 7.5 eV respectively.

By shifting the center of Si plasmon peak to 17.5 eV, the residue signal is about 4 % of the total intensity in the range of 5 eV to 26 eV. The residue signal at about 28.5 eV was also observed in this test and it was considered to be the carbon plasmon signal. It is a good fitting.

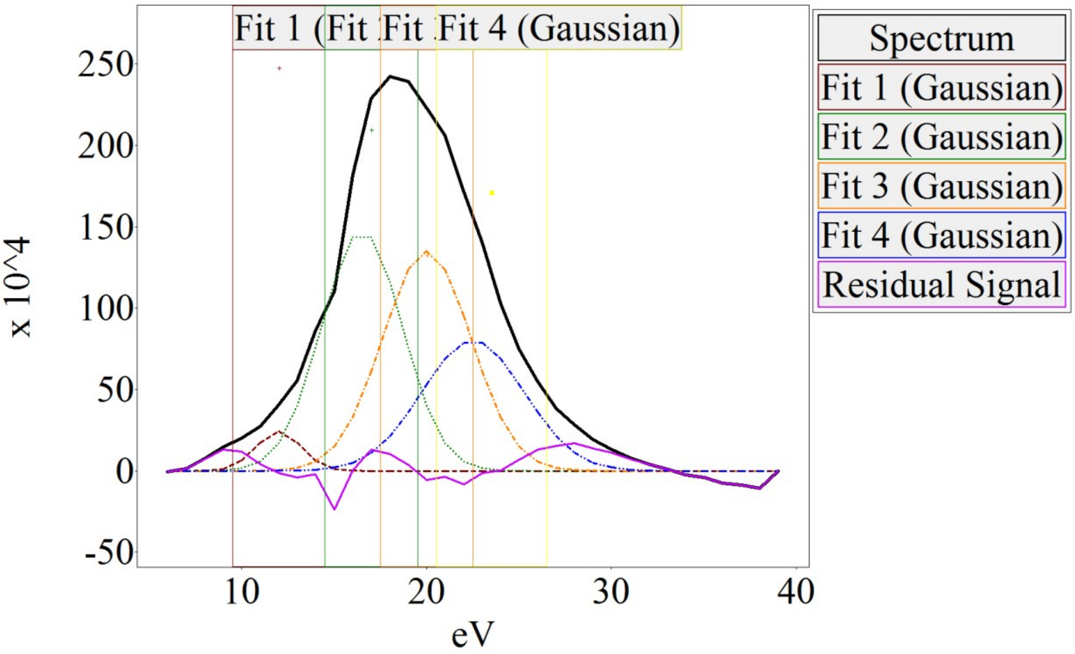

Fig. S6. The fitting results by shifting the center of Si plasmon peak to 16.5 eV. Si surface plasmon, Si plasmon, a-SiC plasmon and 3C-SiC plasmon peaks were represented by the Gaussians 1, 2, 3 and 4 respectively. The centers of Si surface plasmon, Si plasmon, a-SiC and 3C-SiC plasmon peaks were fixed at 12 eV, 16.5 eV, 20 eV and 22.5 eV respectively. The FWHM of 3C-SiC plasmon peak was constrained by 6.5 eV and the FWHM for all other plasmon peaks were not constrained in order to achieve minimum residual signal. The fitted FWHM of Si surface plasmon, Si plasmon and a-SiC plasmon peaks are 3.5 eV, 5.7 eV and 5.6 eV respectively.

By shifting the center of Si plasmon peak to 16.5 eV, the residue signal is about 8 % of the total intensity in the range of 5 eV to 26 eV. It is not a good fitting. Therefore, from the above fitting tests, the center of Si plasmon peak was determined to be 17.2 ± 0.3 eV with a FWHM of 5.3 ± 0.3 eV. And the FWHMs for other three plasmon peaks were also obtained from the testing and listed in Table 2.

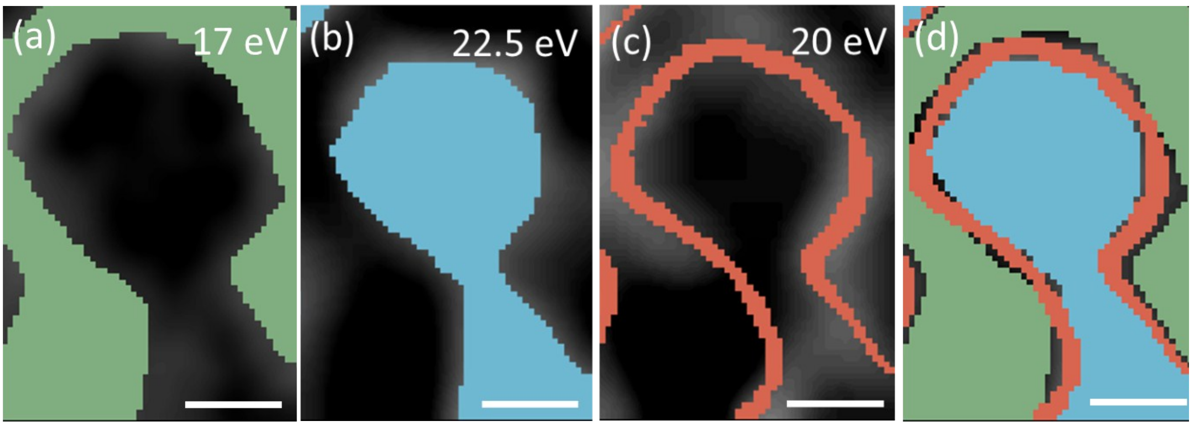

Fig. S7. Segmentations performed on the reconstructed tomograms. The segmentations were applied on the reconstructed tomograms using: (a) Si plasmon signal (in green color), (b) 3C-SiC plasmon signal (in blue color), (c) a-SiC plasmon signal (in red color). A combined segmentation is shown in (d). The scale bars are 5 nm. The segmentation was performed by choosing a threshold intensity at which the contours were represented in colors. In the reconstructed tomograms, the signals themselves have soft outlines, as expected from the delocalization of plasmon scattering.[4] Therefore, we set up a threshold value to avoid choosing the diffused signal (~ 1 nm).

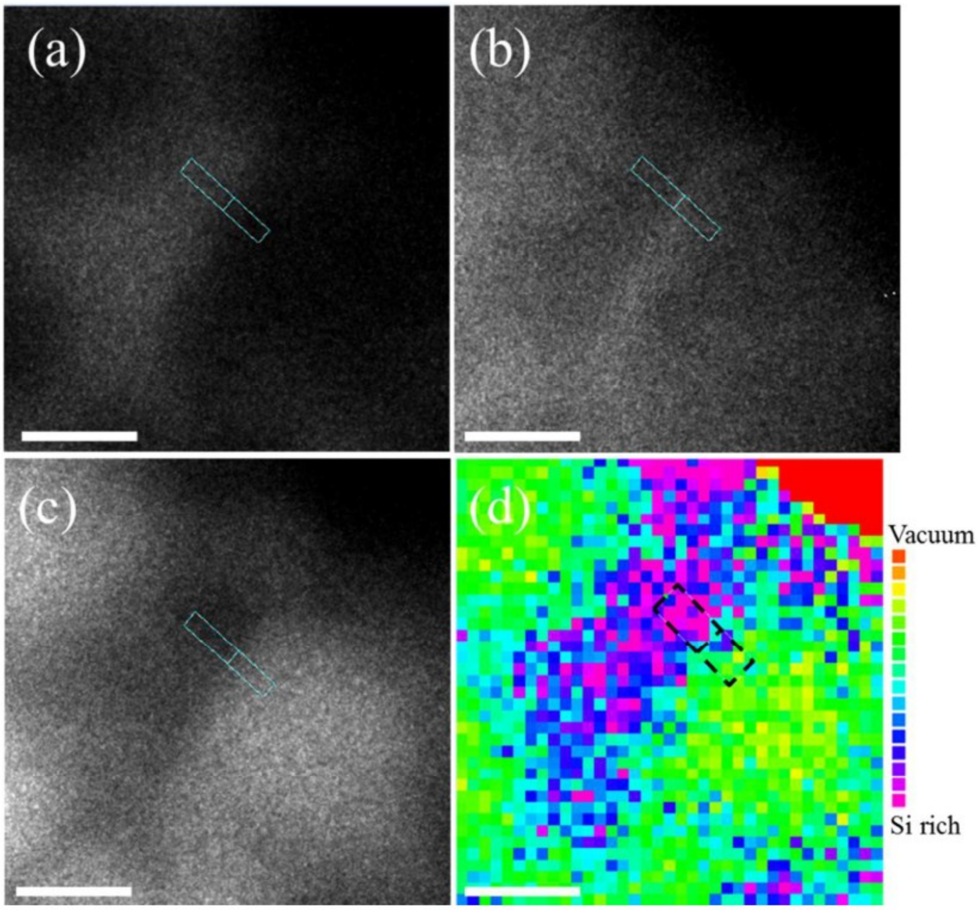

Fig. S8: The compositional fluctuation of Si from the regions of the Si network like structure, a-SiC to 3C-SiC NPs. The plasmon images of Si, a-SiC and 3C-SiC shown in (a), (b) and (c) were acquired from the same area as in (d). The STEM-EELS core-loss mapping in (d) was acquired using the Si-L edge and C-k edge signals to show the compositional fluctuation of Si. The pixel size of the STEM-EELS mapping is 0.5 nm × 0.5 nm. The scale bars are 5 nm. The line in the rectangular marked areas in (a)-(d) indicates the position of the a-SiC interface.

The plasmon images and STEM-EELS mapping were acquired from a region that is thin enough to minimize the overlapping effect of the Si and SiC phases in 2D images. By analyzing the plasmon images of Si, a-SiC and 3C-SiC (Fig. S8 (a)-(c)), a thin a-SiC interface was observed between Si and 3C-SiC regions. In Fig. S8 (d), we observe that the concentration of Si in the a-SiC interface layer is intermediate between the Si network and the 3C-SiC regions.

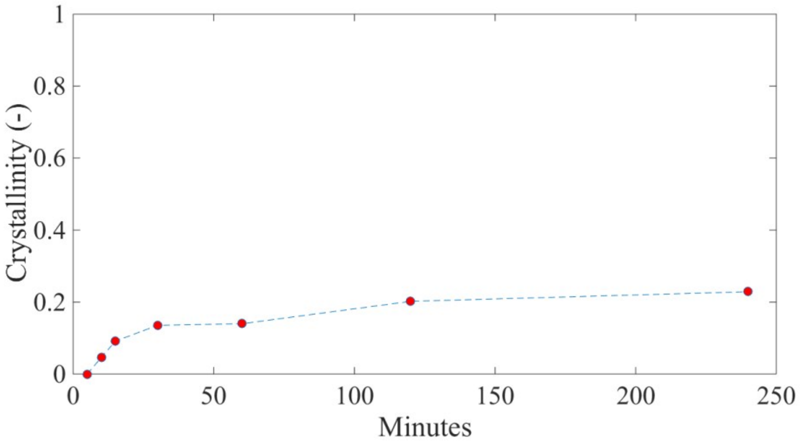

Fig. S9: Raman analysis of the crystallinity of Si volume fraction in the analysed SRSC films as a function of various annealing times (the dashed lines are a guide to the eye).

The Raman Spectroscopy measurement is useful technique to obtain the crystalline fraction in the materials. The method used to obtain the crystalline volume fraction of the materials is called Integrated Raman Fitting Routine (IRFR)[5]. A four phonon mode contribution is used in the IRFR method for the amorphous phase in combination with a modified phonon confinement model to represent the crystalline phase[5]. The phone modes of the amorphous phase are modelled as Gaussian distributions, while the phonon mode of the crystalline phase is described by a phonon confinement mode which represents the transverse optical (TO) mode of the crystalline phase. The crystalline volume fraction is determined by Eq. 1:

$$X_c = \frac{I_{C,TO}}{I_{C,TO} + \gamma I_{A,TO}} \qquad (1)$$

Where X_c is the crystalline volume fraction, $I_{C,TO}$is the area of the crystalline TO peak, $I_{A,TO}$ is the area of the amorphous TO peak, γ is a correction factor for the difference in cross section of c-Si and a-Si: ($\frac{\sigma_{c-Si}}{\sigma_{a-Si}}$), it is set at 0.8 as suggested in many studies[6,7].

The time series measurement results (Fig. 1) obtained from Raman Spectroscopy indicate a rapid increase of the crystalline Si (c-Si) volume fraction (V_{c-Si}) within the first half hour. From half hour to four hours annealing, V_{c-Si} slowly increases from 13% (at half hour) to 22% (at four hours). The abrupt increase of Si-Si crystalline bonds in the first half hour indicates the formation of crystalline Si nanoparticles (NPs). The very small increase of crystallinity established from half hour to four hours annealing indicates that a quasi-steady state has been locally between the precipitated Si NPs and the surrounding amorphous Si (a-Si) matrix. The amorphous Si matrix takes the majority of the volume fraction in the Si network structure through the whole time series at 1100^{o}C.

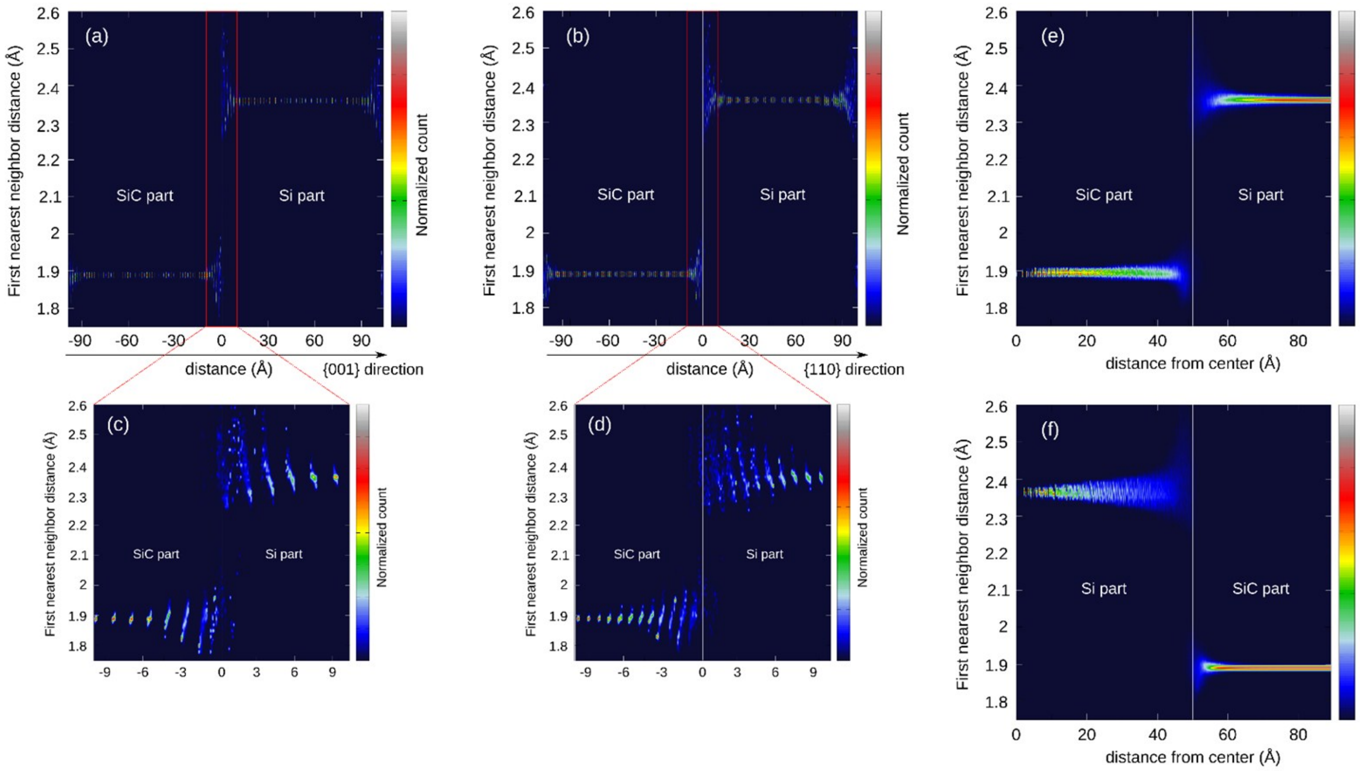

Fig. S10. First nearest neighbour distance as a function of the distance from the interface in the model. (a) {111} interface with 98.7 Å SiC and 104.0 Å Si part along {001} planes; (b) {111} interface with 96.1 Å SiC and 103.5 Å Si part along {110} planes. (c) and (d) show the first nearest neighbour distribution in 1 nm from the interface in both Si and SiC parts (see the red rectangle in (a) and (b)) for models along {001} and {110} planes, respectively. First nearest neighbour distance as a function of the distance from the center of the model with: (e) 50 Å SiC NP embedded in 152.6 Å Si matrix and (f) 50 Å Si NP embedded in 148.41 Å SiC matrix.

We have carried out simulations for larger Si and SiC parts in sizes in order to see the better the length over which the interfacial disorder relaxes. From the simulated results, we observed that the width of interfacial disorder remains unchanged with increasing the size of Si and SiC parts. And, the interfacial disorder extends over 6-8 Å on Si parts and 3-5 Å on the SiC part which can be seen from both Fig.5 in the manuscript and Fig. S10. The total width of interfacial disorder layer is about 1.1 nm which is in a good agreement with the width of the a-SiC layer observed from the 3D analysis.

References:

1 M. Mitome, Y. Yamazaki, H. Takagi and T. Nakagiri, *J. Appl. Phys.*, 1992, **72**, 812–814.

2 M. Kuenle, S. Janz, K. G. Nickel and O. Eibl, *Phys. Status Solidi a-Applications Mater. Sci.*, 2011, **208**, 1885–1895.

3 R. F. Egerton, *Electron energy-loss Spectrosc. electron Microsc.*, 1986, xii+410 pp-xii+410 pp.

4 A. Yurtsever, M. Weyland and D. A. Muller, *Appl. Phys. Lett.*, 2006, **89**, 151920.

5 M. V. De Grunt, "Raman spectroscopy of silicon quantum dots embedded in a silicon carbide matrix," Mater's thesis, Delft University of Technology, 2013.

6 R. Tsu, J. Gonzalez-Hernandez, S. S. Chao, S. C. Lee and K. Tanaka, *Appl. Phys. Lett.*, 1982, **40**, 534–535.

7 M. van Sebille, J. Allebrandi, J. Quik, R. A. C. M. M. van Swaaij, F. D. Tichelaar and M. Zeman, *Nanoscale Res. Lett.*, 2016, **11**, 355.